Characterization of gas hydrate from geophysical data the region of Tumbes-Progresso Basin (PERU)

Zoraida Tejada and Ellen Gomes, Programa de Pós-graduação em Geofísica (UFPA)

Abstract

Gas hydrate is known as a potential source of hydrocarbon energy. However, the detection and exploration of this resource is still inexpressive. This is due to two factors: the difficulty of detecting profitable areas of gas hydrate and the high risk involved in exploration. In this study, an analysis is presented to detect possible areas of gas hydrate occurrence in a region of the Tumbes-Progresso Basin (PERU) using geophysical data: magnetic, gravity, seismic, and well data. The study consists of three approaches to demarcate the possible zones of hydrate: First, magnetic and gravity anomalies were analyzed with respect to the geology to choose a study area. This analysis was followed by seismic imaging of the region of interest to identify potential gas hydrate based on the presence of BSRs (Bottom Simulating Reflectors), and this BSR potential was applied to an AVO analysis (Amplitude Versus Offset). Finally, in the third approach, well data were evaluated, calculating the porosity and saturation of the rock in the Gas Hydrate Stability Zone (GHSZ). The probable occurrence of gas hydrate in the study area was verified based on the results of the analysis.

Introduction

Gas hydrates are compounds formed by gas molecules encapsulated by "cages" of frozen water that are stable in shallow regions with systems of specific pressure and temperature (SLOAN, 1998; KENNETT, CANNARIATO, *et al.*, 2003). In other words, gas hydrate is gas trapped in ice.

The use of geophysical data in the detection of gas hydrates on a large scale has been achieved through observed seismic reflection in the appearance of seismic profiles from a strong reflector of negative amplitude and sub-parallel to the seabed, known as the BSR.

There are specific characteristics in the regions where gas hydrate is formed. Peru is a country with a high probability of having gas hydrate reserves, but there is still little known of its occurrence in the region. Specifically, results of a marine survey conducted in 2010 by Karoon Gas Australia company, in the Tumbes-Progress Basin of Peru indicate the presence of gas hydrate in Block Z-38. However, Karoon Gas Australia is unaware of commercially viable deposits.

This paper presents applied geophysical data, such as gravity, magnetic, seismic, and well data, for the analysis of gas hydrates occurring in the Tumbes-Progress Basin.

Method

The area of interest is located southeast of Tumbes-Progress Basin and northeast of Talara Basin on the northern Peru continental shelf, seaward of the coasts of the provinces of Zarumilla, Tumbes, and Contralmirante Villar (see Figure 1). The pull-apart Tumbes-Progress Basin has been affected by the movement and interaction of tectonic plates since the Early Cretaceous. The source rocks of the basin correspond to a marine clastic sequence known as the Heath Formation, and reservoir rocks are sandstones belonging to the Zorritos Formation.

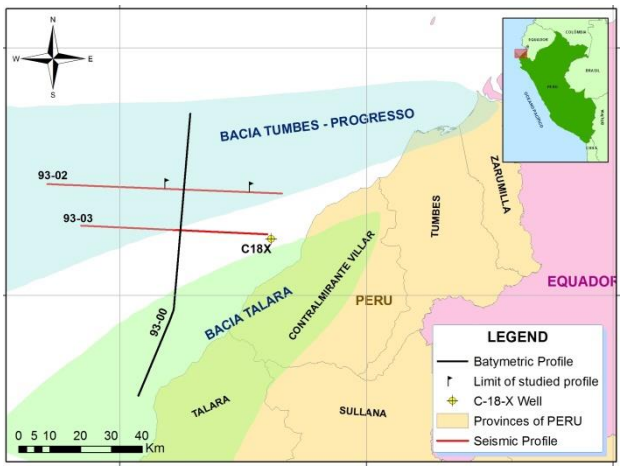

Figure 1: Location Map of Tumbes-Progress Basin.

Geophysical data were provided by the PERUPETRO S.A. Company, including two 2D seismic lines from the RIB93 marine survey, magnetic and gravimetric maps acquired in 2009, and well logs from 1979. To detect possible areas of occurrence of gas hydrates, we analyzed the geophysical data in the following sequence:

- Analysis of magnetic and gravity anomalies to choose the area of the basin to be studied.
- Selection of the study area through seismic imaging analysis and identification of possible reflectors associated with gas hydrates and free gas.
- Application of AVO analysis to potential reflectors.
- Evaluation of gas hydrate in the Gas Hydrate Stability Zone (GHSZ) from well data.

I - Analysis of magnetic and gravity anomalies.- The magnetic anomalies depend on the existence of ferromagnetic particles of rocks. In rocks with gas hydrate, salt water occupying the pore spaces dilated in the formation store methane and create a favorable

environment for bacteria to feed in due to the high flow of methane. Oxidation of methane produces electrons. Minerals such as iron oxide and sulfide are reduced when receiving these new electrons. Without the layers of low permeability, the flux migrates and spreads throughout formation above the BSR reflector, leading to a complete pyritization and resulting in decreased signals of the ferromagnetic particles such as iron sulfide (ESTEBAN e ENKIN, 2008). Effects of demagnetization also occur. In the study region, demagnetization at low latitudes (inclination of the geomagnetic field in the area is approximately 15°) generated a positive anomaly that is higher compared to anomalies of neighboring regions.

Based on a magnetic map of the basin, it can be observed that there are anomalies ranging from -18 to 5nT (Figure 2a). Areas with a higher positive anomaly, and therefore with greater probability of gas hydrate, are identified in Figure 2a as Areas 1, 2 and 3.

These areas are also shown on the 3D Bouguer anomaly map (Figure 2b). This map shows a lateral variation of density in the Tumbes-Progress Basin in which there are three areas of interest. We can note high density values when Area 1 and Area 2 refer to the basement of the basin. While in Area 3, the presence of negative anomalies corresponds to the basin itself.

Based on analysis of magnetic and gravimetric maps and a priori information, we have determined that in Area 1, the magnetic anomaly refers to the behavior of Banco Peru (PERUPETRO, 2005), It is an isolated basement of intermediate mafic composition that generally has a low content of silica, potassium, and sodium and high MgO and FeO. The anomaly of Area 2 corresponds to the structural depression developed over the local crust (PERUPETRO, 2005), which is characteristic of a basin generated by transtensional slip faults. In Area 3, the anomaly is the deepest base of the basin (see Figure 2). We concluded that Area 3 is the most suitable area for the potential occurrence of gas hydrates, and therefore, this area was chosen for the analysis.

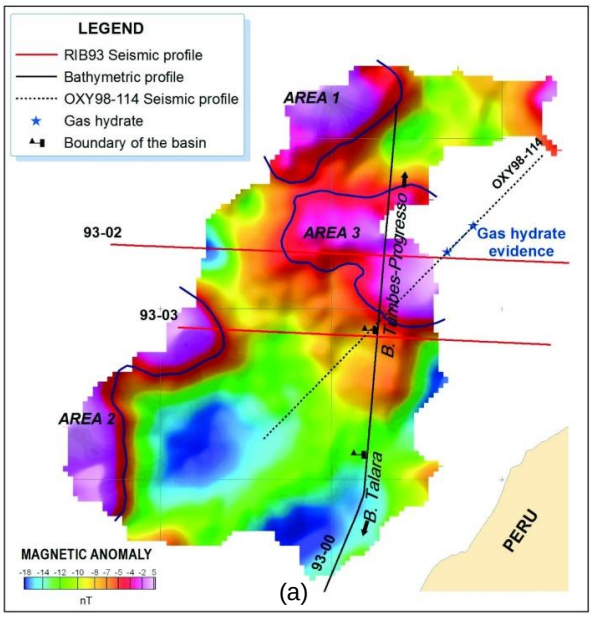

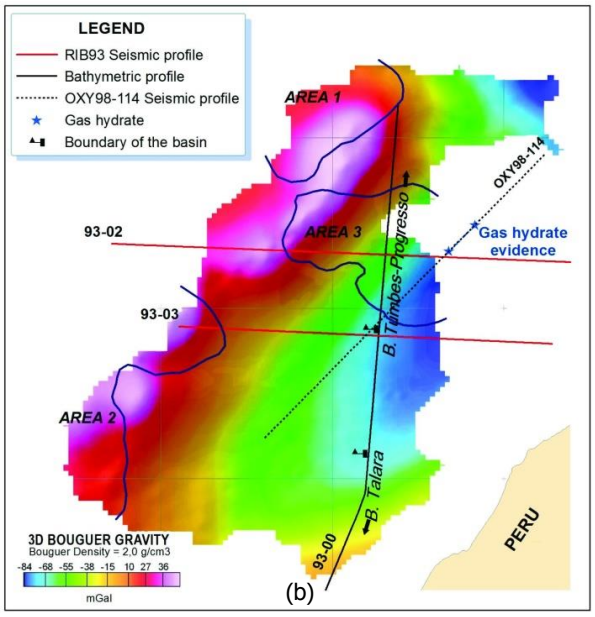

Figure 2: (a) Magnetic map and (b) Bouguer gravity anomaly map acquired in 2009 by Karoon Gas Australia Company. Areas with the highest probability of occurrence of gas hydrates are identified as Area 1, Area 2, and Area 3. The magnetic map also shows where there is evidence of gas hydrates.

II - Selection of an area by seismic imaging analysis.- Seismic lines RIB93-02 and RIB93-03 were acquired in 1993 in the marine survey RIBDGC93LZ. The interval between sources is 25m, and the number of receivers is 168, with an interval of 25m. The minimum offset is 277m, and the maximum offset is 4452m. The observation time is 8 seconds, with a sample interval of 2ms. The goal was to generate a section migrated in time for identification of reflector-type BSR. While the marine line indicates surface multiple reflections that would justify processing to mitigate these multiple reflections, this processing was not applied because our purpose was to apply methodologies that maintain the signal amplitude, and this attenuation can implicate AVO analysis. Spherical divergence correction does not affect the AVO analysis as verified.

The preprocessing consisted of performing geometry corrections according to the field report, which allowed for editing traces and applying amplitude correction for spherical divergence. Preprocessing was followed by velocity analysis. The RMS velocity has variations of 1480 m/s to 5000m/s. Additionally, there were high velocity values measured in the first few meters below the seafloor, contradicting the expected behavior of seismic velocity increasing with depth. This is due to a geological crust that was deposited in the Quaternary known as terraces. This phenomenon is best observed in places where the water depth is shallow (approximately 120 to 250ms). An NMO correction was made using the velocity map, stacking and then post-stacking migration in time. (See Figure 3 and Figure 4) Potential reflectors of type BRS are marked by green curves. These were chosen based on the depth and continuity of the reflector.

Two regions were marked, based on line RIB93-02 shown in Figure 3. In the first region, between CDPs 2500 and 2800, the reflector of interest appears with a time of 1000ms and cuts the multiple of surface of first order. Due to its location away from the depocenter of the basin, this type of reflector suggests an intra-basin BSR. The second region, between CDPs 2920 and 3100, also suggests a BSR intra-basin type reflector.

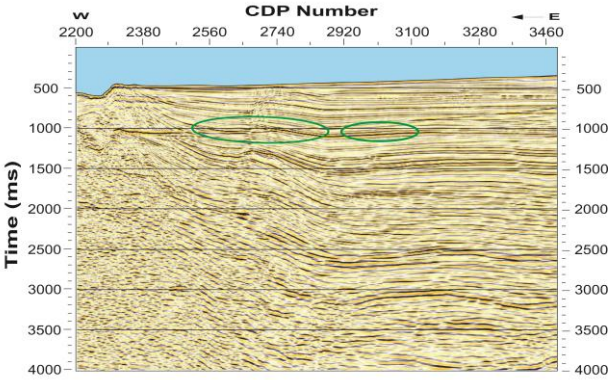

Figure 3: Seismic section post-stack migrated in time for line RIB93-02. BSR potential is highlighted by green curves.

In Figure 4, four distinct regions were marked based on line RIB93-03. The first is between CDPs 168 and 617, where the reflectors of interest appear between 600 and 1200ms. If it is confirmed as a BSR reflector, it would be ridge type of Class IV. In the second region between CDPs 617 and 1397 and 1000 and 1300ms of time, several dipping structures are identified, suggesting BSR intra-basin type reflectors; however, they are not parallel to the seafloor due to tectonic activity of the basin (KAROON, 2009; KVENVOLDEN e KASTNER, 1990; HERBOZO, HÜBSCHER, *et al.*, 2013). The third and fourth regions are located between CDPs 1675 and 1917 and CDPs 2177 and 2440, respectively, and suggest BSR intra-basin-type reflectors.

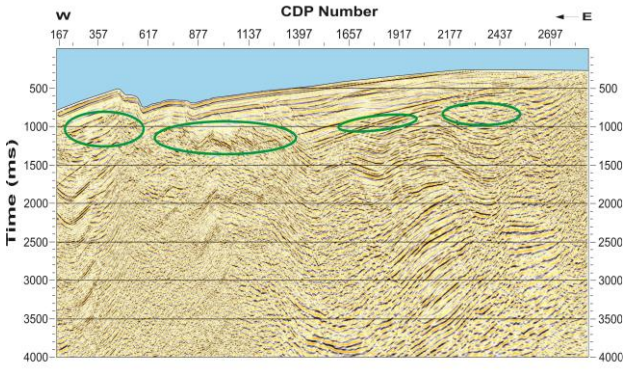

Figure 4: Seismic section post-stack migrated in time for line RIB93-03. BSR potential is highlighted by green curves.

III - Application of AVO analysis to potential reflectors.- A detailed analysis is necessary to confirm that the identified reflectors discussed above are the type BSR. This can be done by AVO analysis. The analysis is the variation of seismic reflection amplitude with change in distance between the source and the receiver, which indicates differences in lithology and fluid content in rocks above and below the reflector. The study of this variation is called AVO analysis, and this is based on calculations using Zoeppritz (1919) equations. Through this analysis, one can estimate the thickness, porosity, density, velocity, lithology, and fluid content of the rocks. An approximation for the reflection coefficient of the P wave, considering angles of incidence smaller than 30° is given by (SHUEY, 1985).

$$R(\theta) = A + B\,sin^2(\theta) \tag{1}$$

with

$$\mathrm{A} = R_0 \quad \text{or} \quad \mathrm{A} = \frac{1}{2}\left(\frac{\Delta V_p}{V_p} + \frac{\Delta\rho}{\rho}\right) \tag{2}$$

and

$$B = \left(A_0 R_0 + \frac{\rho}{(1-\rho)^2} \right) \quad \text{or}$$
$$B = -2\frac{V_s^2}{V_p^2}\frac{\Delta\rho}{\rho} + \frac{1}{2}\frac{\Delta V_p}{V_p} - 4\frac{1}{2}\frac{V_s^2}{V_p^2}\frac{\Delta V_s}{V_s} \tag{3}$$

where $R(\theta)$ is the reflection coefficient, θ is the angle of incidence, A is the intercept, $\mathrm{R_o}$ is the reflection coefficient given normal incidence, B is the gradient, A_o specifies the normal decrease gradually in amplitude with offset, and $\Delta\sigma$ contrasts the Poisson ratio; V_P and V_S is the P and S-wave velocity of the medium of incidence, ΔV_P and V_S are contrast of the P and S-wave velocity at the interface, r is the density of the incident medium and Δr is the density contrast at the interface, V_{int} is the interval velocity, V_{rms} is the velocity of root mean quadratic, T_o is the time to normal incidence and X is the distance.

The method to calculate the angle of incidence from the interval and RMS velocity is described by:

$$\sin(\theta) = \frac{V_{int}}{V_{rms}}\left(\frac{X}{X^2 + (V_{rms}T_0)^2}\right) \tag{4}$$

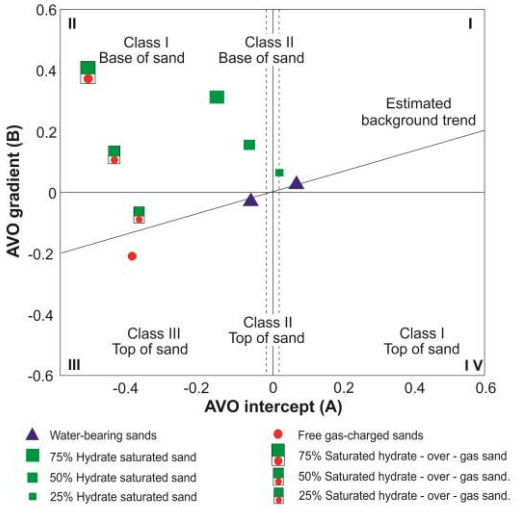

Figure 5: AB Plane and AVO class – numeration of the quadrants is proposed by Rutherford and Williams (1989), and the results are proposed by Zhang et al. (2012).

The AVO method is intended to obtain the values of A and B for different events. These values determine a plot

called the AB plane. The horizontal axis of the AB plane refers to the values of A, and the vertical axis refers to values of B. The AB plane divides space into four quadrants. Each pair of AB values determines a point that will belong to one of the quadrants (RUTHERFORD e WILLIAMS, 1989) present a classification of AVO anomalies, according to their locations in the AB plane. There are three classes (Figure 5):

- Class 1: A positive and B negative. Reservoirs that have higher impedance than the surrounding rocks.
- Class 2: A near zero, with B negative. Reservoirs with very small impedance contrasts, both positive and negative.
- Class 3: A and B negative. Reservoirs of low impedance.

To determine reflectors from possible BSRs, a polygon was created within the section gradient attribute (B). Anomalies with values of A and B are shown inside the polygon in the AB plane, but a new polygon was created in Quadrant II in the AB plane where, according to previous analyses of Zhang et al. (2012) the anomalies of gas hydrate are found in different degrees of saturation and type. Finally, attribute values A and B of Quadrant II of the AB plane are shown in, Figure 6b and Figure 7b (green points), or each selected reflector, the behavior of the amplitudes with offsets intercepting the results in the AB plane was analyzed. The goal was to find deviations in the general trend or background in the behavior values of A and B. Deviations in the background can be indicators of lithology or fluid contente (RUTHERFORD e WILLIAMS, 1989; CASTAGNA, SWAN e FOSTER, 1998; KIM, KIM, *et al.*, 2011; SARMENTO, 2005).

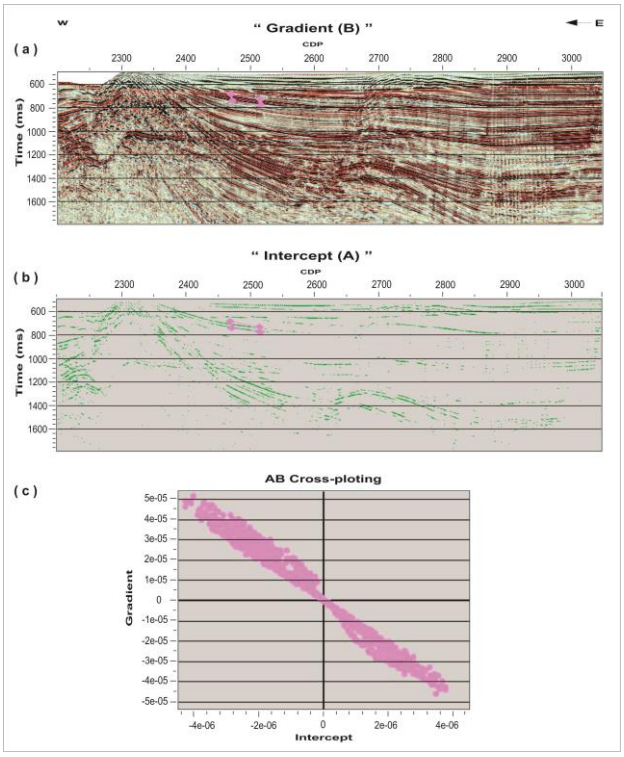

Figure 6: Analysis of gradient (B) and intercept (A) attributes of line RIB93-02. Between CDPs 2450 and 2510, for a reflector with time of approximately 650 ms (marked by the polygon in magenta). (a) Selected values of B for the reflector of interest (within the polygon in magenta) are shown in the section of gradient attribute (B). (b) For the values of B within the blue polygon in Figure 6b, the reflector to be studied is now shown inside the magenta polygon. (c) AB plane anomalies associated with the values of A and B of the reflector of interest. The anomalies are distributed in a line across Quadrants II and IV of the AB plane.

In line RIB93-02 (Figure 6) the reflector located between CDPs 2450 and 2510 with time of 700ms was analyzed and showed a moderate angle to the ocean floor. Anomalies A and B plotted on the AB plane (magenta dots) in Figure 6c follow a linear trend cutting Quadrants II and IV of the AB plane. This behavior is characteristic of lithologic change or multiple reflections and is therefore an unlikely indicator of the presence of gas hydrate.

The next reflector analyzed (Figure 7) of RIB93-03 line, is located between CDPs 950 and 990 with time of approximately 1210ms. According to Figure 7c spread anomalies in the AB plane are shown in Quadrant II and fit into the classification presented in Zhang et al. (2012) as Class I. These may represent anomalies with different degrees of gas saturation. Thus, this region presents probable occurrence of gas hydrate and a BSR reflector.

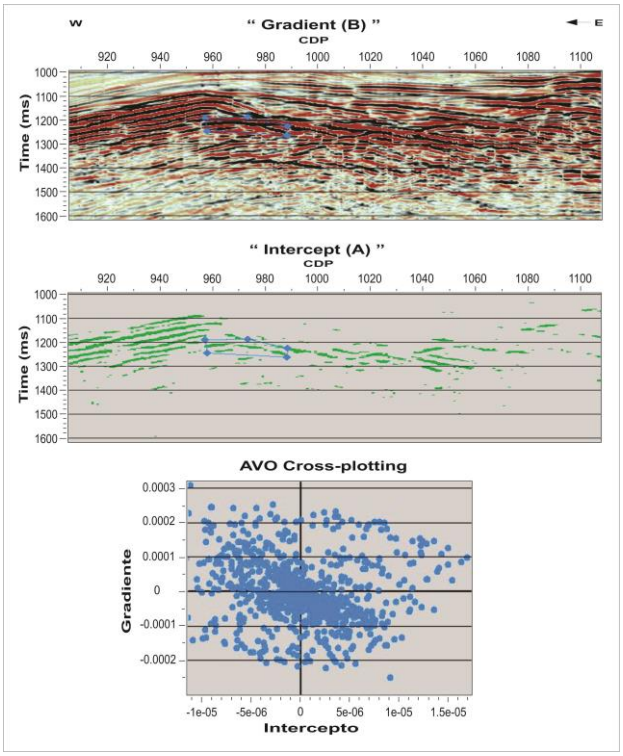

Figure 7: Analysis of gradient (B) and intercept (A) attributes of line RIB93-03. The reflector analyzed is located between CDPs 950 and 990 with time of approximately 1210ms. (a) A blue polygon is marked in the section of gradient attribute (B) to highlight the reflector of interest. (b) The values of B belonging to Quadrant II of the AB plane are shown in green, and the reflector of interest is located within the blue polygon. (c)

AB plane with anomalies related to the values of A and B inside of the blue polygon (blue dots).

IV - Evaluation of gas hydrate in the GHSZ from well data.- Well Z1A-65-14XC (C-18-X) is located 2km from seismic line RIB93-03, within the "Piedra Redonda" Field in the Progress-Tumbes Basin. Gas hydrate can be detected through the analysis of conventional well log data due to its high velocity sonic profile and high resistivity in the electrical resistivity profiles. (MAJUMDER, 2009; COLLETT e LADD, 2000). The profiles analyzed were caliper, gamma ray, resistivity, density, and sonic.

The analysis of the profiles was made to a depth of 1220m (equivalent to approximately 1422ms) considering this as the probable depth of the GHSZ. The objective was to determine the distribution and deposition of hydrate.

Initially, we analyzed the gamma ray log, Figure 8, with the goal of identifying regions where there is no shale, considering the possibility of finding hydrate in sandstones. The next step was to analyze the caliper log in sandstones saturated with hydrate, which shows significant variation and may indicate unconsolidated sediment. Considering that hydrate, like ice, acts as an electrical insulator, the resistivity profile was evaluated in comparison with the other two profiles chosen, which resulted in the identification of four zones (see Figure **8**). Zone 1 is approximately within the range of 433m to 506m, Zone 2 extends from 533m to 634m, Zone 3 extends from 686m to 838m, and Zone 4 ranges from approximately 945m to 1097m. The zones are shown as blue bands in Figure 8.

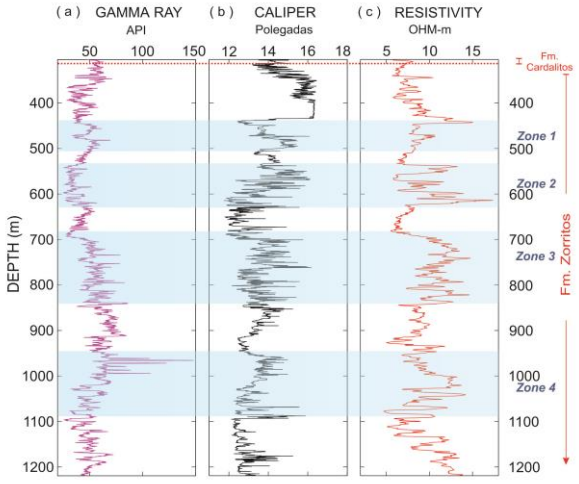

Figure 8: Profiles from well Z1A-65-14XC (C-18-X) and areas analyzed. Zones 1, 2, 3, and 4 are marked by blue bands

According to analyses of the zones, Zone 2 is more likely to contain hydrate concentrations. It has low concentration and high porosity and is formed by thin layers of medium to coarse-grained sandstone with thin interbedded shale, which are characteristics of the Zorritos Formation. At depths of 552 and 576m, the non-shale indicates a favorable porosity and low water saturation; these characteristics are maintained at a depth of 597m (Figure 9). The plot of velocity data versus gamma ray data shows higher values of 1870m/s (velocity of free gas) in the non-shale interval, according to Naresh and Sanjeev (2011) the minimum value of velocity attributed to gas hydrate is 1989m/s. Based on our analyses, there was no basis for considering Zones 1 and 3, and for Zone 2, there will probably be an occurrence of gas hydrate distributed in disseminated form. The same characteristics are shown in the lower part of Zone 4.

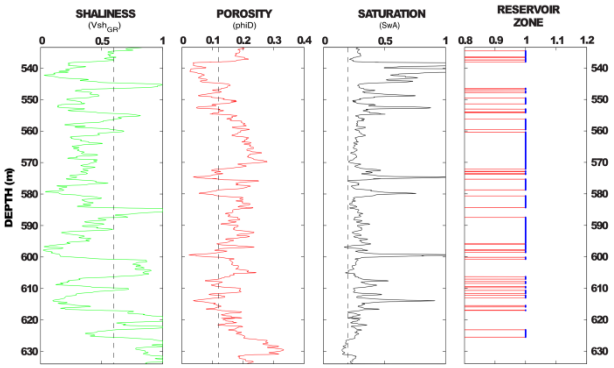

Figure 9: Evaluation of training in Zone 2 in the range of 533 to 634m in well Z1A- 65-14XC (C-18-X). The data for shaliness, porosity, and saturation are calculated using the Archie formula (GLOVER, 2010; KIRK, 1995). The reservoir zone is determined from the data shaliness, porosity, and saturation according to Masoudi et al. (2012).

Results

Based on the results of the analysis of seismic imaging, AVO analysis, and the well logs, it has been concluded that there are areas in the vicinity of seismic lines RIB93-03 and RIB93-02 (Figure 10) where the occurrence of gas hydrate is likely. Identified probable BSRs in the RIB93-03 migrated time section are shown in Figure 11, The BSRs are highlighted in magenta. The BSRs are identified in the time range of 1000 to 1300ms. All BSRs are identified as intra-basin type because they are farther away from the margin of the basin and closer to the depocenter. As shown in Figure 11, two types of BSR reflectors have been identified for line RIB93-03. The first is between CDPs 617 and 1397 with time of 1000 to 1300ms. In the figure, there are several dipping structures suggesting reflectors of intra-basin type that are not parallel to the seafloor. It is believed that this is due to the tectonic activity of the basin (KAROON, 2009; HERBOZO et al., 2013). Studies of Karoon Gas Australia Company identified a BSR with the same behavior in a time of approximately 1500ms, corresponding to the Zorritos Formation, in an area close to line RIB93-03. The second BSR reflector is between CDPs 1675 and 1917 and suggests a BSR intra-basin reflector of thermogenic origin. For line RIB93-02 between CDP 2500-2800 and time 1000ms, the BSR presented the same behavior as the line RIB93-03 reflectors. All of these reflectors have been identified in seismic imaging as probable BSRs, which were confirmed by AVO analysis.

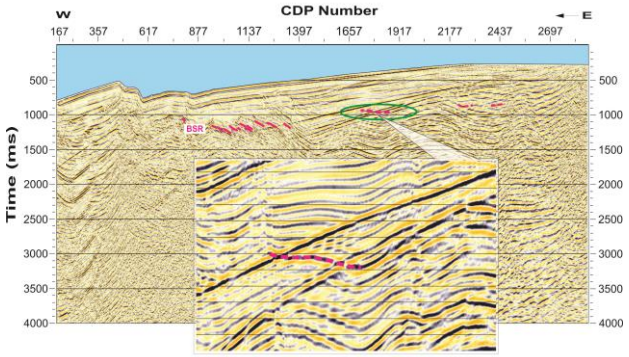

Figure 10: Migrated time section of the RIB93-02 line. BSR identified and marked in magenta. Highlighted in the region of the BSR.

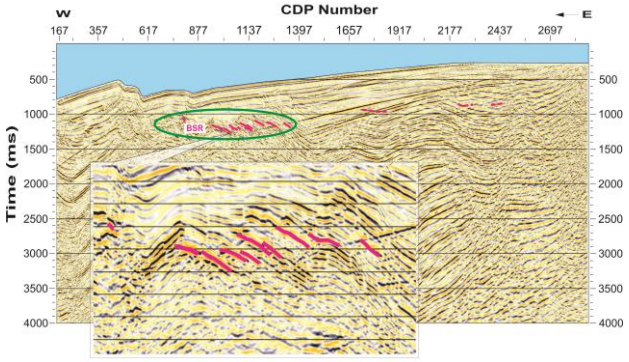

Figure 11: Migrated time section of the RIB93-03 line. BSR identified and marked in magenta. Highlighted in the region of the BSR.

Conclusions

In this study, we tried to contribute information with the identification of areas of probable occurrence of gas hydrate in an area of the Tumbes-Progresso Basin through the use of geophysical data. This identification was made using gravity, magnetic, seismic, and borehole data.

The choice of the probable gas hydrate area within the Tumbes-Progresso Basin was made through the analysis of the magnetic anomaly map. It was verified in the gravity anomaly map because gravity anomalies are insensitive to the presence of gas hydrate. Seismic imaging methods were applied to the probable area to identify BSR potential, and it is concluded that the basin was subject to subsidence regimens during the pull-apart basin evolution, indicating BSRs with intra-basin type thermogenic origin. AVO analysis was then applied to the study area, which verified the probable presence of gas hydrate; specifically type Class I in Quadrant II of the AB plane. BSRs were found at an approximate depth of 1000 to 1100ms. Gas hydrate occurs as disseminated grains in the GHSZ.

Geologically, it is known that the region of interest of hydrate is in the Zorritos Formation, from 330m to 1583m (KAROON, 2009). According to petrophysical interpretation studies of Karoon (2009), the Mancora Formation is composed of 95.6% methane gas at 3,400m. Therefore, it is possible that the gas hydrate is of thermogenic origin (tertiary migration) due to the composition and origin of the gas (HERBOZO, HÜBSCHER, *et al.*, 2013).

The application of new technologies in seismic acquisition is recommended for a better delimitation, evaluation, and estimation of potential fields of gas hydrate, as well as seismic acquisitions through 4C Ocean-bottom seismometers (OBS) and application of Marine Controlled-source Electromagnetic (MCSE) methodology.

Acknowledgments

Thanks to the PERUPETRO S.A Company for providing us with geophysical data to develop this investigation.
I am most grateful to CNPq and Postgraduate Geophysics Courses (CPGf) at Federal University of Pará (UFPA) for permitting the first author to conduct this study. Thanks to PhD teacher João Batista Corrêa de Silva for sharing your knowledge, discussions, and suggestions.

References

ESTEBAN, L.; ENKIN, R. J. Gas hydrate and magnetism: comparative geological setting for diagenetic analysis. International conference Gas Hydrate 6th. Canada: [s.n.]. 2008. p. 6-10.
HERBOZO, G. et al. Influence of recent depositional and tectonic controls on marine gas hydrates in Trujillo Basin, Peru Margin. Marine Geology, p. 30-48, 2013.
HUI, D. et al. Seismic data processing and the charaterizatin of gas hydrate bearing zone offshore of southwestern Taiwan. Terrestrial, Atmospheric and Oceanic Sciences, December 2006. 781-797.
KAROON, E. I. Perú Block Z-38: end of first term interpretation report. Lima, p. 248. 2009.
KENNETT, J. P. et al. Methane hydrates in quaternary climate change: the clathrate gun hypothesis. 2000 Florida Avenue, N. W. Washington: American Geophysical Union, 2003.
KVENVOLDEN, K. A.; KASTNER, M. Gas hydrate of the peruvian outer continental margin. Proceeding of the ocean drilling program, 1990. 10.
PERUPETRO, S. A. Tumbes and Talara Basin Hydrocarbon Evaluation. Lima. 2005.
RUTHERFORD, S. R.; WILLIAMS, R. H. Amplitude-versus-offset variations in gas sand. Geophysics, v. 54, p. 680-688, 1989.
SHUEY, R. T. A Simplification of the zoeppritz equations. Geophysics, v. 50, p. 609-614, April 1985.
SLOAN, E. D. Clathrate hydrates of natural gases. New York: Marcel Dekker Inc., 1998.
ZHANG, Z.; MACONNELL, D. R.; HAN, D.-H. AVO crossplot analysis in unconsolidated sediments containing gas. SEG, December 2012.
ZOEPPRITZ, K. VII b. about reflection and passage of seismic waves through discontinuity surfaces. Mathematics and Physical Class, 1919. 66-68.